Journal of Photochemistry & Photobiology, A: Chemistry 443 (2023) 114836

Contents lists available at ScienceDirect

Journal of Photochemistry & Photobiology, A: Chemistry

journal homepage: www.elsevier.com/locate/jphotochem

Computational design of covalently bound dimers for singlet fission

Davide Accomasso [a,*], Nadia Ben Amor [b], Maurizio Persico [a], Giovanni Granucci [a]

[a] Università di Pisa, Dipartimento di Chimica e Chimica Industriale, via Moruzzi 13, 56124 Pisa, Italy
[b] Université Paul Sabatier, Laboratoire de Physique et Chimie Quantiques, 118 route de Narbonne, 31062 Toulouse, France

ARTICLE INFO

Keywords:
Singlet fission
Covalent dimer photophysics
Computational design
Diphenyl-isobenzofuran
Diamino-fluoroquinone

ABSTRACT

We present two different computational approaches to design covalently bound dimers for singlet fission. Both designs aim at maximizing the effective coupling between the initial singlet excited state S^* and the double triplet state TT, by tuning the interaction (mainly through-space) between the chromophore units. Design I is based on a preliminary search for the optimal relative arrangements of chromophores in a space of possible stacked pair geometries. Then, the optimized dimeric arrangements are used as targets for the covalent connection of the two chromophores. In design II, all viable ways to covalently bind the two chromophores are considered, using a given set of linkers. Next, the most promising covalent dimers for singlet fission, among our tested candidates, are identified. The application of our approaches to a locked 1,3-diphenyl-isobenzofuran chromophore and a diamino-fluoroquinone compound allowed to design several promising dimers for singlet fission, featuring large S^*-TT effective couplings and favorable energetics.

1. Introduction

Singlet fission (SF) is a photophysical process observed in molecular materials in which a singlet excited state S^* is split into two triplet excitons ($T + T$) [1–4]. The possibility for the two triplets to form an overall singlet state (TT) makes SF a spin-allowed process and hence potentially very fast, often occurring in the sub-picosecond time scale [5,6]. The utilization of SF in photovoltaic devices represents a promising strategy to overcome the Shockley–Queisser efficiency limit of about 1/3 [7], and reach a maximum theoretical efficiency of nearly 1/2 [8].

The first requirement for efficient SF is that the isolated chromophore unit satisfies specific energetic conditions, the most important of which requires that two times the triplet energy $\Delta E(T_1)$ is below the energy of the lowest singlet excited state $\Delta E(S_1)$ [1]. However, once a compound which fulfills the aforementioned energy criteria has been found, the SF efficiency is highly sensitive to the mutual disposition of chromophores in the actual material [9]. Specifically, the relative chromophore orientation and distance affect not only the energy of the initial singlet state S^*, but also the coupling of S^* with the double triplet state TT and the other states involved in the SF mechanism. Among the latter, low-lying charge transfer (CT) states are of paramount importance since they may promote SF either via a mediated mechanism or by acting as real intermediates in a two-step route [10]. The role of CT states in the SF mechanism mainly depends on their energies, which in turn are highly sensitive to the chromophore mutual arrangement and to the environment.

To date, most of the studies on SF have focused on molecular crystals, where SF is intermolecular in nature and its efficiency is highly dependent on the crystal packing and morphology [11–14]. However, the realization of specific intermolecular arrangements in the solid phase represents a very difficult task. In this regard, covalent dimers, i.e. systems where two chromophore units are covalently bound together, appear to be more suitable. In particular, in this kind of systems, where SF is intramolecular in nature, the highly controllable covalent bonding can be exploited to attain specific interchromophore arrangements.

As pointed out in a recent review [15], besides the more controllable mutual disposition of chromophores, covalent dimers offer additional potential advantages over molecular crystals. Specifically, in addition to the through-space interaction between chromophores, the linkers could provide through-bond coupling that may facilitate intramolecular SF. Moreover, covalent dimers offer a greater control over the surrounding environment. This can be used to better exploit the effect of the CT states on SF, by tuning their energy with the variation of the dielectric environment, without affecting the interchromophore coupling. Furthermore, the intrinsic intramolecular SF should not be altered by the attachment of covalent dimers to charge- or energy-harvesting materials. Therefore, covalent dimers are of interest for implementation of new photovoltaic devices in which they are adsorbed as individual units on a semiconductor support.

A large variety of covalently bound dimers has been already proposed for SF, using different SF compounds as chromophore units and

* Corresponding author.
E-mail address: davide.accomasso@dcci.unipi.it (D. Accomasso).

https://doi.org/10.1016/j.jphotochem.2023.114836
Received 11 March 2023; Received in revised form 25 April 2023; Accepted 8 May 2023
Available online 11 May 2023

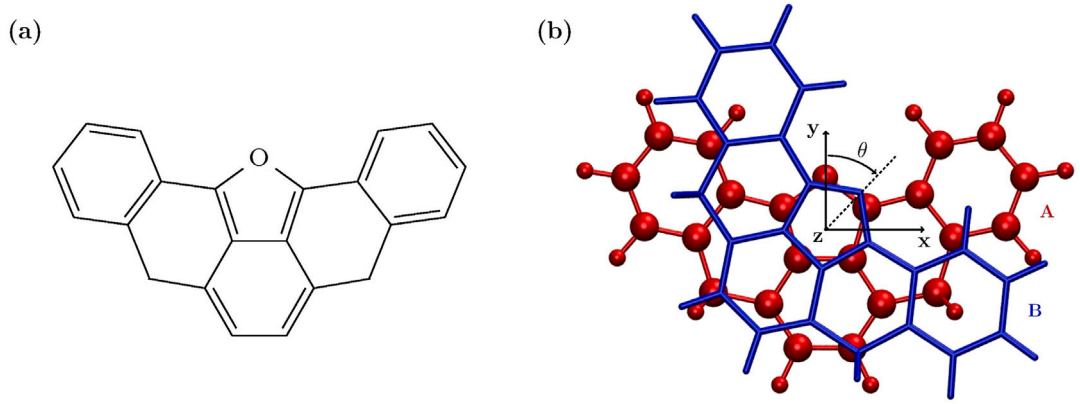

Fig. 1. (a) Molecular structure of methylene-locked 1,3-diphenyl-isobenzofuran (ML-DPBF). (b) Dimer model of ML-DPBF employed in the search for the optimal dimeric arrangements. Molecule A is fixed, while molecule B is rotated about the z axis of an angle θ, and translated along the x and y axes.

a wide selection of linkers. Most of the effort has been dedicated to the synthesis and characterization of covalent dimers of tetracene [16–24] and pentacene [22,24–32]. Additionally, covalent dimers of 1,3-diphenyl-isobenzofuran (DPBF) [33–35], aromatic diimides [36,37], perylene [38], quinoidal thiophenes [39,40], azaborine-substituted compounds [41,42], BODIPY [43], pyrene [44], and diphenylhexatriene [45] were designed and studied with regard to SF. Most of these investigations were focused on fine-tuning the through-bond coupling between chromophores by testing different combinations of linkers and connecting sites [16–18,22,23,25–30,33,35,41,42,45], while fewer studies were dedicated to the optimization of the through-space interaction [19,20,24,36–38].

Here, we present two different computational designs of covalent dimers for SF. Our design approaches are based on the maximization of the effective electronic coupling between the initial singlet state S^* and the double triplet state TT, by fine-tuning the through-space interaction between the two chromophore units. The effective coupling is quantified by means of a diabatization procedure, based on the localization of molecular orbitals and electronic states [46]. In design I (Section 2), we first identify the optimal mutual dispositions of chromophores in a three-dimensional space of possible stacked pair geometries. Then, the two chromophores are covalently bound together so as to attain the optimized dimeric arrangements. In design II (Section 3), we consider several ways to covalently connect the two chromophores, using different linkers. Next, the most promising covalent dimers for SF, among our tested candidates, are identified. We present our design approaches as applied to a locked 1,3-diphenyl-isobenzofuran chromophore and a diamino-fluoroquinone compound, both recently proposed for SF on the basis of their monomer properties [47].

2. Design I: Covalent dimers of a locked 1,3-diphenyl-isobenzofuran

Our first design of covalent dimers involves a search for the mutual dispositions of two chromophores which optimize SF. Our search is based on the maximization of the effective electronic coupling between the initial singlet state S^* and the double triplet state TT in a space of possible slip-stacked dimers. The optimized dimeric arrangements are then used as target arrangements to covalently bind together the two chromophores.

This design approach is suitable for SF chromophores featuring several possible connecting sites and a planar molecular geometry. As an example, we applied our approach to the methylene-locked 1,3-diphenyl-isobenzofuran (ML-DPBF) chromophore (Fig. 1a).

2.1. Search for the optimal dimeric arrangements

Our proposed search for the optimal mutual dispositions of two chromophores requires to perform electronic structure calculations at a very large number of dimeric geometries and represents a very expensive computational task for any high quality ab initio method. To reduce the computational cost, we used the semiempirical R-AM1/FOMO-CASCI(4,8) method in which the parameters were previously optimized for the ML-DPBF compound (for computational details, see Section 2.3).

In our search for the optimal mutual dispositions of chromophores in a dimer, we used a model system consisting of two equivalent molecules of ML-DPBF, each at the R-AM1/FOMO-CASCI(2,4) optimized S_0 geometry (point group C_{2v}), placed on parallel planes at a distance of 4.0 Å. We chose this value because it approximately corresponds to the interplane distance of the isobenzofuran groups (~3.8 Å) in the slip-stacked dimers that can be extracted from the two crystalline forms of 1,3-diphenyl-isobenzofuran (DPBF) [13], the parent compound of ML-DPBF. In this way, we reduced the full six-dimensional space of mutual arrangements and limited our search to only three degrees of freedom. They are two translations of molecule B along the x and y axes and one rotation of the same molecule about the z axis, i.e. the axis perpendicular to the molecular plane and passing through its center of mass (see Fig. 1b).

Our proposed optimization procedure aims at finding the local maxima of the following function:

$$F(\Delta x, \Delta y, \theta) = \sqrt{\langle S_1 S_0 | \hat{H}_{el}^{eff} | TT \rangle^2 + \langle S_0 S_1 | \hat{H}_{el}^{eff} | TT \rangle^2} \quad (1)$$

where Δx and Δy are the translation distances along the x and y axes, θ is the rotation angle of one molecule relative to the other, and $\langle S_1 S_0 | \hat{H}_{el}^{eff} | TT \rangle$ and $\langle S_0 S_1 | \hat{H}_{el}^{eff} | TT \rangle$ are the effective electronic couplings between $S_1 S_0$ or $S_0 S_1$ and TT states, respectively. The latter include both the direct coupling between $S_1 S_0$ or $S_0 S_1$ and TT states, and the contribution from higher-lying states, which in our model are the charge transfer states $A^- B^+$ and $A^+ B^-$, and the high-energy localized excitations $S_2 S_0$ and $S_0 S_2$ (for more details, see Section 2.3).

The local maxima of function F (Eq. (1)) were determined using the following procedure. First, we evaluated F on a grid in which Δx and Δy were varied from −6.0 to 6.0 Å and from −5.0 to 5.0 Å, respectively, by increments of 0.25 Å, while θ was varied from 0° to 180°, by increments of 15°. The rotation interval was limited to [0°, 180°] for symmetry reasons. Then, we identified a set of geometries possibly close to local maxima of F by comparing nearest-neighbor points of the grid. Subsequently, starting from these geometries, the local maxima of F were further refined by maximization of function F using the simplex method [48].

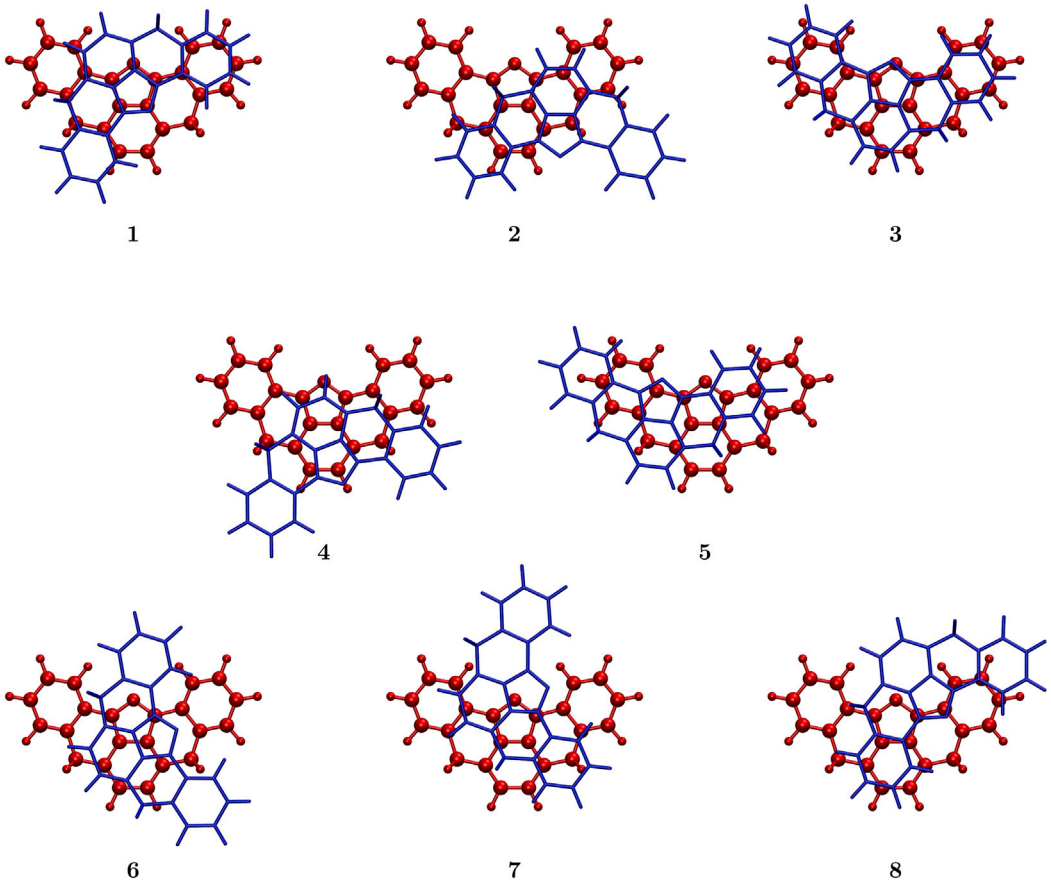

Fig. 2. The first 8 optimal dimer arrangements of ML-DPBF, obtained as local maxima of F (Eq. (1)). Atomic coordinates are provided in Section S4.1.

Table 1
Electronic couplings and energy differences for the first 8 optimal dimer arrangements of ML-DPBF (see Fig. 2). The latter are local maxima of function F, defined in Eq. (1). The reported electronic couplings and energies are computed using the R-AM1/FOMO-CASCI(4,8) method.

	Δx	Δy	θ	Coupling (meV)		Energy gap (meV)[c]			
	(Å)	(Å)	(deg.)	F[a]	D[b]	$S_2^* - S_1^*$	$TT - S_1^*$	$TT - S_2^*$	$CT_1 - S_2^*$
1	0.039	−0.102	140.7	37.3	4.5	379.0	412.9	33.9	182.5
2	2.581	−2.337	180.1	27.6	4.7	259.1	331.1	72.0	459.0
3	−0.481	0.146	9.2	27.3	4.8	495.6	462.7	−32.9	118.7
4	0.563	−2.981	158.6	24.4	4.8	335.5	385.9	50.4	404.9
5	−2.585	0.155	6.6	23.0	2.9	316.1	387.9	71.7	299.9
6	1.101	−0.752	68.5	22.3	3.1	132.1	297.1	165.0	354.2
7	0.478	1.808	76.2	22.2	2.2	138.3	302.5	164.2	339.5
8	1.941	1.630	141.1	21.4	3.1	241.6	344.9	103.4	311.7

[a] F is defined as $\sqrt{\langle S_1S_0|\hat{\mathcal{H}}_{el}^{eff}|TT\rangle^2 + \langle S_0S_1|\hat{\mathcal{H}}_{el}^{eff}|TT\rangle^2}$ (Eq. (1)), and quantifies the effective coupling of the S_1S_0 and S_0S_1 states with TT, including the effect of CT states A^-B^+ and A^+B^-.

[b] D is defined as $\sqrt{\langle S_1S_0|\hat{\mathcal{H}}_{el}|TT\rangle^2 + \langle S_0S_1|\hat{\mathcal{H}}_{el}|TT\rangle^2}$, and quantifies the direct coupling of the S_1S_0 and S_0S_1 states with TT.

[c] Energy gap between states i and j (i.e. $i - j$) defined as $E_i - E_j$. A positive gap indicates that state i is above state j, while a negative gap means that i lies below j. State notation: S_2^*, S_1^*, higher- (bright) and lower-energy (dark) excitonic states, respectively; TT, double triplet state; CT_1, lower-energy state of charge transfer character.

The grid of points in which function F was evaluated is reported in Figure S5 in the form of contour maps. The first 20 "crude" maxima identified in the grid were used as starting geometries for optimization, from which we obtained 10 distinct local maxima. The best 8 optimized dimer arrangements are shown in Fig. 2. The corresponding values of F are provided in Table 1, together with the combined $S_1S_0/S_0S_1 - TT$ direct coupling (D) and selected energy gaps between excitonic states (see end of Section 2.3 for the definition of the excitonic basis). For all dimers **1**-**8** the excitonic state S_2^* is the bright combination of S_1S_0 and S_0S_1 (Table S8), and hence it will be the most populated state upon photoexcitation.

We see in Table 1 that dimer **1** shows by far the largest effective interaction between S_1S_0/S_0S_1 and TT (F). However, the largest $S_1S_0/S_0S_1 - TT$ direct couplings are observed in dimers **3** and **4**. From Table 1 we also notice that for dimers **1**-**5** the $TT - S_2^*$ energy gap is very small (< 0.1 eV), while it is slightly larger (0.1–0.2 eV) for dimers **6**-**8**. Interestingly, in dimer **3** the TT state is slightly below S_2^*, while in all the other dimers in Fig. 2 TT is energetically above the S_2^* state. Dimer **3** also shows the smallest energy gap between S_2^* and the lowest charge transfer state CT_1. These two features of dimer **3** can be mainly attributed to the large $S_2^* - S_1^*$ splitting (∼ 0.5 eV), which in turn is due to the strong interaction between S_1S_0 and S_0S_1. Such effect also

implies a large $TT - S_1^*$ gap at the Franck–Condon region, which might be detrimental to SF in case of an initial ultrafast $S_2^* \rightarrow S_1^*$ transfer of population, since it may slow down the subsequent $S_1^* \rightarrow TT$ transition.

Some of the optimal dimers of ML-DPBF identified in this work are very similar to already proposed dimeric arrangements of the parent compound DPBF [49]. In particular, dimers **1** and **2** in Ref. [49] resemble our dimer **6**, and dimers **4** and **5** reported in [49] are very similar to our dimers **7** and **5**, respectively. However, we also noticed important divergences between the two proposed sets, which can be due to the structural differences between DPBF and ML-DPBF (at variance with ML-DPBF, DPBF is not planar, due to the twisting of the phenyl rings out of the plane of the isobenzofuran core) and, to a greater extent, to the different definition of the maximization function. In fact, while in the present work we optimized the effective electronic coupling between S_1S_0/S_0S_1 and TT (Eq. (1)), the search in Ref. [49] is based on the maximization of the SF rate constant, evaluated using Marcus theory.

Moreover, our identified optimal dimers of ML-DPBF can be compared with the crystalline dimeric arrangements of the DPBF derivatives investigated in Ref. [50]. Among our optimal mutual dispositions, only dimers **3** and **5** (Fig. 2) partly resemble the slip-stacked dimers **2**, **6**-**8** of the fluorinated DPBF compounds investigated in Ref. [50], while all the other optimal dimers of ML-DPBF in Fig. 2 differ significantly from the reported crystal structures [50]. This suggests that fluorination of ML-DPBF might be unsuitable for the realization of our optimal dimeric arrangements in molecular crystals and, therefore, alternative strategies of crystal engineering would be required.

2.2. Covalent dimers preparation and characterization

Optimal dimeric arrangements **1**-**3** (Fig. 2) were then selected as targets for covalently linking the two ML-DPBF chromophores. In the preparation of covalent dimers, the choice of connecting sites in the two monomers was mainly dictated by the target dimeric arrangement. Moreover, the linkers were selected so as to fulfill the following conditions: (i) the stacking distance between the two chromophores in the covalent dimer is close to 4 Å; (ii) π conjugation via the linkers, which may affect the SF energetics, is avoided; (iii) the linkers are sturdy enough and do not introduce any photostability issue. With these aims, we selected the ether chains -O-$(CH_2)_m$-O- ($m = 1, 2$) as our linkers.

For each selected optimal arrangement we tested two ways to link the chromophore pair, which differ in the position, length and number of the linkers. We call the covalent dimers **Dn** and **Dn'**, **n** = **1**-**3**, where **n** refers to the corresponding optimal dimeric arrangement. In Fig. 3 we show our designed covalent dimers of ML-DPBF, each at its ground state geometry optimized using the R-AM1/FOMO-CASCI(4,8) method (for details, see Section 2.3). Side views of the same covalent dimers are shown in Figure S6. The dimeric geometries obtained are better characterized and compared with the corresponding optimal arrangements in Table 2, in which we also reported the effective and direct couplings, F (Eq. (1)) and D, and relevant energy gaps between excitonic states. We see that in all covalent dimers the stacking arrangement is retained, with interchromophore distances between ~3.5 and ~3.8 Å. Moreover, the mutual dispositions of chromophores in the designed covalent assemblies are close to the corresponding target dimeric arrangements.

In covalent dimer **D1** we used two -O-$(CH_2)_2$-O- bridges to covalently link the two chromophore units. We see from Table 2 that, while the interchromophore orientation in **D1** is very close to the target arrangement **1**, the slip distance (r) between chromophores is larger in **D1**, compared to dimer **1**. This results in a decrease of both F (from 37.3 to 23.2 meV) and D (from 4.5 to 1.1 meV). The introduction of a third -O-$(CH_2)_2$-O- linker, leading to dimer **D1'**, appears to be beneficial for the $S_1S_0 - TT$ and $S_0S_1 - TT$ couplings. In fact, **D1'** shows large F and D values, despite the mutual disposition of chromophores does not differ much from the one in dimer **D1**. This suggests that small geometrical changes in **D1** may be sufficient to obtain important increases of F and D. In Table 2 we also see that the energy separation between TT and the bright excitonic state S_2^* is slightly larger in dimers **D1** and **D1'** (~ 0.06 eV), compared to **1** (~ 0.03 eV), and the $CT_1 - S_2^*$ energy gap is significantly smaller in both **D1** and **D1'**. The $S_2^* - S_1^*$ and $TT - S_1^*$ energy separations in **D1** and **D1'** are instead very close to corresponding gaps in dimer **1**.

Similarly to dimer **D1**, two -O-$(CH_2)_2$-O- chains were used in the first attempt to covalently connect the chromophores of target dimer **2**. In the resulting covalent dimer **D2** (Fig. 3) the optimal interchromophore orientation of dimer **2** is satisfactorily attained. However, despite a significantly shorter interchromophore distance (~3.5 Å), dimer **D2** shows much smaller $S_1S_0 - TT$ and $S_0S_1 - TT$ couplings (see their F and D values in Table 2) and a larger $TT - S_2^*$ energy separation, compared to **2**. However, in **D2** we also have a much smaller $CT_1 - S_2^*$ gap, and the $S_2^* - S_1^*$ and $TT - S_1^*$ energy differences are very close to the ones in **2**. This situation does not differ much in the alternative dimer **D2'**, in which the two chromophores were linked using two -O-CH_2-O- bridges (see Fig. 3). As we can see in Table 2, dimer **D2'** shows even smaller $S_1S_0 - TT$ and $S_0S_1 - TT$ couplings and a much larger $CT_1 - S_2^*$ energy gap, compared to **D2**.

Two additional covalent dimers were designed starting from the optimal dimeric arrangement **3**. As for **D1** and **D2**, we used two -O-$(CH_2)_2$-O- linkers for each dimer. Moreover, two different combinations of connecting sites were tested, leading to dimers **D3** and **D3'** (Fig. 3). We see that the target interchromophore orientation **3** is approximately attained in **D3** and **D3'**, and both dimers show large $S_1S_0 - TT$ and $S_0S_1 - TT$ couplings (see F and D values in Table 2). However, as in dimer **3**, the $S_2^* - S_1^*$ Davydov splitting is quite large. As a consequence, the TT and S_2^* states are very close in energy, while a large energy gap (~0.5 eV) separates TT from S_1^*. As already mentioned in Section 2.1, a large $TT - S_1^*$ gap might be detrimental for SF, since it can hinder the $S_1^* \rightarrow TT$ transition. We also notice that in **D3** and **D3'** the CT_1 state is quite low in energy, and in **D3** it lies below the bright excitonic state S_2^*.

To better assess the SF energetics, we have optimized the geometries of our designed dimers for their adiabatic S_1 state (referred to as S_1^d). For all our ML-DPBF dimers, the TT state is the lowest excited state at the S_1^d minimum, i.e. TT becomes the lowest excited state upon geometry relaxation (Table S9). This suggests that, even if population rapidly funnels to the lowest excitonic state S_1^*, the subsequent transition from S_1^* to TT is energetically favored in our dimers. Moreover, since our electronic structure methodology includes all the important stabilization effects of S_1^*, i.e. excitonic coupling, mutual polarization and mixing with the CT states [51], we can conclude that the energy relationships of the S_1^*, S_2^* and TT states are reasonably well assessed.

Overall, our designed covalent dimers of ML-DPBF represent promising systems for intramolecular SF. In each dimer, the mutual disposition of chromophores at the optimized ground state geometry is very close to the corresponding target dimeric arrangement. Moreover, all designed covalent dimers show quite large $S_1S_0 - TT$ and $S_0S_1 - TT$ effective couplings ($F \geq 5$ meV) and very small energy gaps between the bright excitonic state S_2^* and TT (< 0.15 eV). The largest values for the effective coupling F (Eq. (1)) are obtained for dimers **D3'** and **D1'**. However, these dimers show quite large $S_2^* - S_1^*$ energy splittings (~ 0.4–0.5 eV), which may slow down SF, in spite of the process being exothermic (Table S9). In this regard, dimers **D2** and **D2'** appear to be more suitable, since their $S_2^* - S_1^*$ and $TT - S_1^*$ energy gaps are smaller (~ 0.2–0.3 eV). Moreover, the use of equivalent connecting sites for the two monomers in dimers **D1**, **D2** and **D2'** should make their synthesis easier, compared to **D1'**, **D3** and **D3'**.

2.3. Computational details of design I

The electronic structure calculations for different arrangements of a dimer model of methylene-locked 1,3-diphenyl-isobenzofuran (ML-DPBF) were performed using a semiempirical configuration interaction

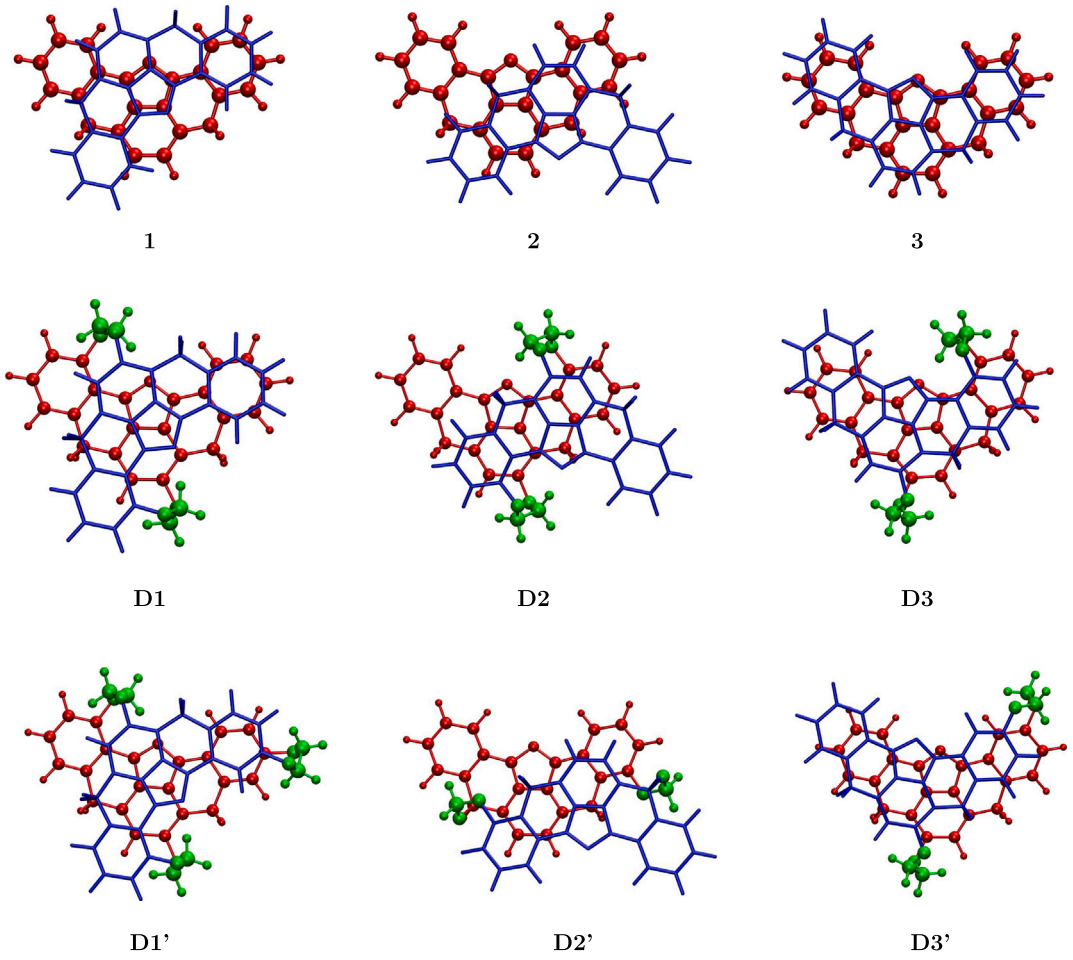

Fig. 3. Covalent dimers of ML-DPBF. The two monomers are shown in red and blue colors, while the linkers are in green. Side views of covalent dimers are shown in Figure S6. Atomic coordinates are provided in Section S4.2. Target dimeric arrangements **1**-**3**, already introduced in Section 2.1, are also shown.

Table 2
Electronic couplings, energy differences and geometrical parameters for covalent dimers of ML-DPBF (see Fig. 3), computed using the R-AM1/FOMO-CASCI(4,8) method. For comparison, the corresponding values for optimal dimeric arrangements **1**–**3** (Fig. 2) are also reported.

	R[a]	r[b]	ϕ[c]	θ[d]	Coupling (meV)		Energy gap (meV)[g]			
	(Å)	(Å)	(deg.)	(deg.)	F[e]	D[f]	$S_2^* - S_1^*$	$TT - S_1^*$	$TT - S_2^*$	$CT_1 - S_2^*$
1	4.000	0.092	0.0	140.7	37.3	4.5	379.0	412.9	33.9	182.5
D1	3.697	1.184	0.3	138.4	23.2	1.1	384.3	445.3	61.0	101.0
D1'	3.802	0.994	3.9	131.0	46.7	5.1	358.9	428.4	69.5	85.2
2	4.000	3.470	0.0	180.1	27.6	4.7	259.1	331.1	72.0	459.0
D2	3.536	3.589	0.0	180.0	8.6	0.5	234.4	381.1	146.7	264.4
D2'	3.687	4.614	2.3	181.3	4.9	0.5	175.3	316.9	141.6	596.0
3	4.000	0.504	0.0	9.2	27.3	4.8	495.6	462.7	−32.9	118.7
D3	3.634	1.249	0.7	19.0	20.3	3.9	496.7	543.4	46.7	−47.4
D3'	3.606	2.169	1.7	9.5	48.1	6.3	427.9	483.4	55.5	36.3

[a] R is the stacking distance between monomers and is defined as the average distance (in Å) between the centroid of one monomer and its projection to the best-fit plane of the other monomer.

[b] r is the slip distance between monomers and is defined as the average distance (in Å) between the centroid of one monomer and the centroid projection of the other monomer to the best-fit plane of the first monomer.

[c] ϕ is the tilting angle and is defined as the angle (in degrees) between the normal vectors of the best-fit planes for the two monomers.

[d] θ is the (relative) rotation angle about the pseudo z axis (Fig. 1) and is defined as the angle (in degrees) between the C_2 axis of monomer A and the projection of the C_2 axis for monomer B onto the best-fit plane of monomer A.

[e] F is defined as $\sqrt{\langle S_1S_0|\hat{H}_{el}^{eff}|TT\rangle^2 + \langle S_0S_1|\hat{H}_{el}^{eff}|TT\rangle^2}$ (Eq. (1)), and quantifies the effective coupling of the S_1S_0 and S_0S_1 states with TT, including the effect of CT states A^-B^+ and A^+B^-.

[f] D is defined as $\sqrt{\langle S_1S_0|\hat{H}_{el}|TT\rangle^2 + \langle S_0S_1|\hat{H}_{el}|TT\rangle^2}$, and quantifies the direct coupling of the S_1S_0 and S_0S_1 states with TT.

[g] Energy gap between states i and j (i.e. $i - j$) defined as $E_i - E_j$. A positive gap indicates that state i is above state j, while a negative gap means that i lies below j. State notation: S_2^*, S_1^*, higher- (bright) and lower-energy (dark) excitonic states, respectively; TT, double triplet state; CT_1, lower-energy state of charge transfer character.

method, with parameters specifically optimized for the system under study. In particular, we employed a configuration interaction method based on floating occupation molecular orbitals (FOMO-CI) [52,53], in its complete active space version (FOMO-CASCI), using an active space of 4 electrons in 8 orbitals, i.e. CAS(4,8), and the AM1 [54] form of the semiempirical Hamiltonian. The AM1 parameters for carbon and oxygen atoms, as well as the Gaussian energy width for floating occupation, were optimized for ML-DPBF so as to reproduce a set of data computed by higher level methods. In this target set we included both properties of the isolated ML-DPBF monomer and data concerning selected dimeric arrangements. Such target data were obtained by DFT/TD-DFT calculations for the monomer [47], and using an excitation selected ab initio MR-CI method for three dimeric arrangements (see Section S1.1). More details on the semiempirical parameterization for ML-DPBF are provided in Section S1.2. In Sections 2.1 and 2.2, this reparametrized semiempirical methodology has been referred to as R-AM1/FOMO-CASCI(4,8).

For each covalent dimer of ML-DPBF presented in Section 2.2, the ground state geometry was optimized at the semiempirical FOMO-CASCI(4,8) level, using the reoptimized AM1 (R-AM1) parameters, presented in Section S1.2, for the ML-DPBF monomers and the original AM1 parameters [54] for the linkers. Moreover, interatomic potential energy terms of Lennard-Jones (LJ) type were added to correct the R-AM1/FOMO-CASCI(4,8) interaction potential between monomers, using the LJ parameters of the OPLS-AA force field [55] (see Section S1.1 in Ref. [56], for details).

The relevant electronic couplings and energy gaps between states for all dimeric arrangements and covalent dimers of ML-DPBF, introduced in Sections 2.1 and 2.2, were computed using the R-AM1/FOMO-CASCI(4,8) method. In particular, we first computed the energies and wavefunctions for the 8 lowest singlet adiabatic states. Next, (quasi-)diabatic states are determined following a procedure based on the localization of the molecular orbitals (MO) on the two monomers and the subsequent rotation of the adiabatic states in the localized MO basis [46]. The latter transformation matrix is defined so as to maximize the overlaps between the diabatic wavefunctions and a set of reference states, i.e. simple configurations with a well-defined character. Here, we used the same 8 reference states employed for the dimer model of DPBF in Ref. [46]. Specifically, they are prototypes for the following diabatic states: the ground state, S_0S_0, the localized excitations S_1S_0 and S_0S_1, the singlet combination of two triplets, TT, the charge transfer (CT) states A^-B^+ and A^+B^-, and the higher-energy localized excitations S_2S_0 and S_0S_2 (see Figure S2 for a schematic representation). Note that, in the diabatic state notation, the first label (like S_0) refers to monomer A, while the second to monomer B.

Once the adiabatic-to-diabatic transformation matrix is defined, the latter is used, together with the adiabatic state energies, to determine the electronic Hamiltonian matrix in the diabatic basis, whose off-diagonal elements quantify the direct couplings between states. To compute the effective electronic couplings between S_1S_0, S_0S_1 and TT, we defined an effective Hamiltonian matrix in which the model space is defined by S_1S_0, S_0S_1 and TT, and the outer space is spanned by A^-B^+, A^+B^-, S_2S_0 and S_0S_2, as described in Ref. [46]. Moreover, to better characterize our investigated systems, an alternative basis of states, called "excitonic", was computed by diagonalizing separately the electronic Hamiltonian matrix blocks of the localized excitations, S_1S_0 and S_0S_1, and the CT states, A^-B^+ and A^+B^-, giving rise to the excitonic states S_1^* and S_2^*, and CT_1 and CT_2, respectively (note that in each group, S_n^* and CT_n, the states are energy ordered).

All the semiempirical R-AM1/FOMO-CASCI calculations were performed using a development version of the MOPAC code [57].

3. Design II: Covalent dimers of a diamino-fluoroquinone

Our second design approach of covalent dimers is based on the identification of the most promising dimers for SF in a set of possible candidates. In particular, several ways to covalently connect the two monomers are considered, by testing different linkers. Then, the candidate covalent dimers are characterized with regard to SF and the most promising dimers are identified.

The present design approach can be applied to SF chromophores having a limited number of connecting sites and for which only few dimeric arrangements can be attained by covalently linking the two monomers. On the other hand, it does not require the ease of stacking typical of planar aromatic structures, which allows the application of the design approach I. Here, we employed approach II to design covalent dimers of a diamino-trifluoroquinone (DATFQ) chromophore (Fig. 4a). DATFQ represents a promising compound for SF, since it both satisfies the fundamental energy requirement for SF [47] and, at variance with some of the previously proposed diamino-quinones [58, 59], is not prone to possible complications due to the presence of NH groups [60]. Moreover, its small size allows to apply high-quality ab initio computational methodologies, making DATFQ a good model compound.

3.1. Preparation of covalent dimers

Our preparation of candidate covalent dimers aims at the realization of a small number of mutual arrangements of chromophores in the covalent assembly, using different linkers. These target arrangements are selected on the basis of qualitative considerations on the chemical structure of the chosen SF chromophore, with preference for the arrangements which maximize the through-space interaction between chromophores.

In the case of DATFQ (Fig. 4a), we considered one target arrangement, in which the two stacked monomers form an anti-parallel mutual disposition (Fig. 4b). Compared to the parallel stacked dimer, the anti-parallel arrangement allows for a more favorable interaction between the two monomers of DATFQ, the electron-donating amino groups of one monomer facing the electron-withdrawing carbonyl groups of the other monomer, and viceversa. Since the DATFQ compound can exist in two enantiomeric forms, namely isomers R and S, we considered both the anti-parallel stacked dimer in which the two monomers are S enantiomers (SS), and the dimer where one monomer is the R enantiomer and the other monomer is the S form (RS).

Next, the two monomers were covalently bound together using two equivalent linkers, as shown in Fig. 4c. We considered the following linkers: -CH_2-, -S-, -CH_2O-, and -CH_2CH_2-. In the following, we will refer to our covalent dimers as SS-L and RS-L, where L indicates the linker. For the -CH_2O- linker, which is not symmetric, we considered both the dimers in which the amino halves of the monomers are connected to the CH_2 group of the linkers and the hydroquinone sides are linked to the O of the bridges (referred to as SS/RS-CH_2O), and the reverse cases (dimers SS/RS-OCH_2).

As a first test for our candidate linkers, we evaluated the strain energy for dimers RS-L, using the following formula:

$$\Delta E_s = E(D_{LL}) - 2[E(M) + E(L)] \quad (2)$$

where $E(D_{LL})$, $E(M)$ and $E(L)$ are the ground state energies of the covalent dimer, the (isolated) monomer and the linker, respectively. The latter, $E(L)$, is computed as the difference between the energy of the dimer in which the monomers are connected using only one linker, $E(D_L)$, and twice the energy of the monomer, i.e. $E(L) = E(D_L) - 2E(M)$. The strain energies for dimers RS-L, computed at the M06-2X/TZVP level (see Section 3.3 for details), are reported in Table 3, together with relevant geometrical parameters. Except for dimer RS-S, the computed strain energies are below 2 kcal/mol, indicating that the strain caused by the covalent connection in our dimers is not significantly large. In one case, i.e. dimer RS-CH_2O, the computed strain energy suggests that linking the two monomers with two -CH_2O- chains is energetically favored ($\Delta E_s < 0$). From Table 3 we also see that, unlike the other RS-L dimers, in RS-CH_2CH_2 the mutual disposition of the two

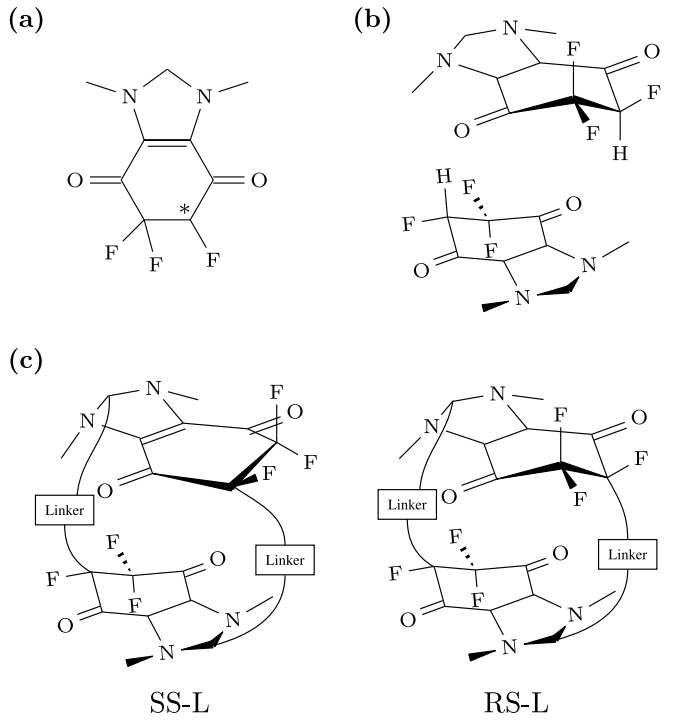

Fig. 4. (a) Molecular structure of the diamino-trifluoroquinone (DATFQ) chromophore considered in our design II. The stereogenic center is marked by a star. (b) Target dimeric arrangement for the preparation of candidate covalent dimers of DATFQ. (c) Schematic representation of our designed covalent dimers of DATFQ. In the SS-L dimer both monomers are enantiomers S of DATFQ, while in RS-L the upper monomer is the R isomer of DATFQ and the lower monomer is the S enantiomer.

Table 3
Strain energies (ΔE_s) and geometrical parameters (R, r and ϕ) for different covalent dimers of DATFQ (Fig. 4c) computed at the M06-2X/TZVP level.

Dimer	ΔE_s[a] (kcal/mol)	R[b] (Å)	r[c] (Å)	ϕ[d] (deg.)
RS-CH_2	1.81	2.826	1.025	0.0
RS-S	5.99	2.911	1.091	0.0
RS-CH_2O	−1.09	4.329	0.485	0.0
RS-OCH_2	0.85	3.851	1.165	0.0
RS-CH_2CH_2	0.88	3.789	1.826	39.5

[a] ΔE_s is the strain energy of the covalent dimer defined according to Eq. (2).
[b] R is the stacking distance between monomers and is defined as the average distance (in Å) between the centroid of the conjugated π system of one monomer and its projection to the best-fit plane of the π system of the other monomer.
[c] r is the slip distance between monomers and is defined as the average distance (in Å) between the centroid of the conjugated π system of one monomer and the centroid projection of the π system of the other monomer to the best-fit plane of the first monomer.
[d] ϕ is the tilting angle and is defined as the angle (in degrees) between the normal vectors of the best-fit planes for the π systems the two monomers.

monomers is quite tilted compared to the target stacking arrangement (monomers on parallel planes, Fig. 4b), the tilting angle between the two monomers (ϕ) being ~ 40°.

From the evaluation of the strain energies and geometrical features of our RS-L dimers, we decided to eliminate -S- and -CH_2CH_2- from our candidate linkers and to focus on -CH_2- and -CH_2O-. Then, we proceeded to characterize the following 6 covalent dimers: SS/RS-CH_2, SS/RS-CH_2O, and SS/RS-OCH_2.

3.2. Characterization of covalent dimers

The molecular structures of our candidate covalent dimers of DATFQ are shown in Fig. 5 (see Figure S8 for side views). These ground geometries, optimized at the M06-2X/TZVP level (see Section 3.3 for more details), are better characterized in Table 4. We see that in our dimers the two monomers are placed on (almost) parallel planes (tilting angle between monomers ϕ ~ 0°), apart from dimer SS-CH_2O ($\phi \simeq$ 24°). In dimers SS/RS-CH_2 the stacking distance (R) between the two monomers is about 2.8 Å, while dimers SS/RS-CH_2O, and SS/RS-OCH_2 show larger values of R (i.e. 3.4 Å < R < 4.4 Å). However, in all our dimers the mutual disposition of the two monomers differs from the perfect (anti-parallel) stacking arrangement. Specifically, the slip distance (r) between monomers exceeds 1.0 Å for dimers RS-CH_2, SS-CH_2O and RS-OCH_2, while it is shorter (< 1.0 Å) for the other three dimers, namely SS-CH_2, RS-CH_2O and SS-OCH_2.

In Table 4 we also reported the $S_1S_0/S_0S_1 - TT$ effective and direct couplings, F (Eq. (1)) and D, and relevant energy gaps between excitonic states for our designed dimers. They were computed at the MR-DDC2 level, with energy shifts determined by comparison with reference (TD-)DFT data for the DATFQ monomer (see Section 3.3 for details). In all our designed dimers, the energy ordering of the lowest excitonic states is $S_1^* < S_2^* < TT < CT_1$, except for dimer RS-$CH_2O$ where TT lies below S_2^*.

Among our dimers, SS-CH_2 shows the largest effective coupling between S_1S_0/S_0S_1 and TT (F), which exceeds 100 meV. In the same dimer, the direct coupling is large ($D \simeq$ 23 meV), and the energy gaps between the higher excitonic state S_2^* and both the double triplet state TT and the lower CT state CT_1 are very small (< 0.15 eV). However, in the same dimer SS-CH_2 the $S_1^* - S_2^*$ and $S_1^* - TT$ energy differences are quite large (> 0.36 eV).

The replacement of one S monomer in SS-CH_2 with its R isomer, resulting in dimer RS-CH_2, leads to a significant decrease in the effective coupling ($F \simeq$ 75 meV), while the direct coupling is almost unaffected ($D \simeq$ 23 meV). This decrease of F, in going from SS-CH_2 to RS-CH_2, can be mainly attributed to the increase in the $S_1^*/S_2^* - CT_1$ and $TT - CT_1$ energy gaps, and to the important decrease in the couplings between TT and the CT states, A^-B^+ and A^+B^-, from ~120 meV to ~47 meV (Table S11). On the other hand, in dimer RS-CH_2 the $S_1^* - TT$ and $S_2^* - TT$ energy gaps are much smaller than in SS-CH_2, the S_2^* and TT states being almost degenerate in RS-CH_2.

Compared to the CH_2-linking, the covalent connection of the monomers with two -CH_2O- chains generally leads to (i) important decreases in F and D, (ii) a significant destabilization of the CT states, and (iii) an important reduction in the $S_1^* - S_2^*$ energy splitting (Table 4). However, in dimers SS-CH_2O and SS-OCH_2, F and D are still quite large, namely for SS-CH_2O $F \simeq$ 43 meV and $D \simeq$ 9 meV, while for SS-OCH_2 $F \simeq$ 32 meV and $D \simeq$ 7 meV. Moreover, in the same two SS dimers the $S_1^* - TT$ and $S_2^* - TT$ energy gaps are small (< 0.35 eV). On the other hand, the corresponding RS dimers, RS-CH_2O and RS-OCH_2, show very small values of F (< 20 meV) and D (< 2 meV). For RS-CH_2O, S_1^* and S_2^* are very close in energy to TT (which is slightly below S_2^*), while for RS-OCH_2 the $S_1^* - TT$ and $S_2^* - TT$ energy gaps are much larger (> 0.4 eV).

Overall, SS-CH_2 and RS-CH_2 are the most promising systems for SF among our candidate dimers, since they show the largest $S_1S_0/S_0S_1 - TT$ effective and direct couplings (F > 70 meV and D > 20 meV), as well as very small $S_2^* - TT$ energy gaps (< 0.15 eV, Table 4). Moreover, in these two dimers the energetic proximity of the CT state CT_1 with S_2^* and TT makes easier its participation in SF through the mediated or two-step mechanisms [1,4], which may promote the formation of TT. Furthermore, although for both SS-CH_2 and RS-CH_2 the TT state is energetically above S_2^* and S_1^* at the ground state geometry, the T_1 and S_1 energies of the DATFQ monomer suggest that the $TT - S_2^*/S_1^*$ energy ordering can be reversed upon geometry relaxation in the excited states [47] (see also below).

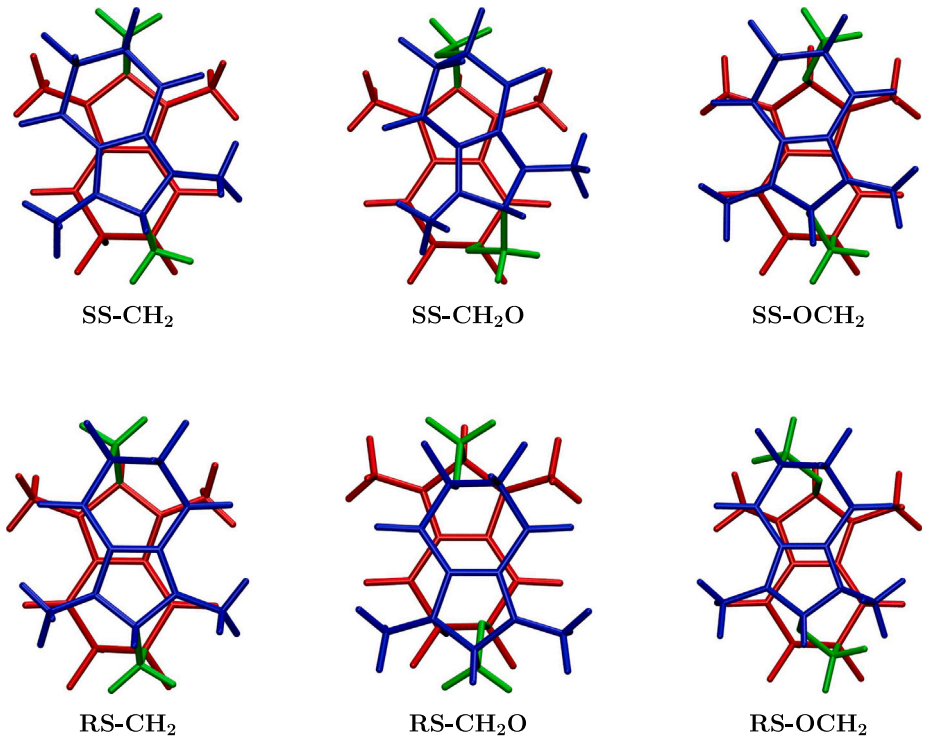

Fig. 5. Covalent dimers of DATFQ. The two monomers are shown in red and blue colors, while the linkers are in green. In dimers RS-L, the upper monomer (blue) is the R enantiomer, while the lower monomer (red) is the S enantiomer of DATFQ. Side views of the same covalent dimers are shown in Figure S8. Atomic coordinates are provided in Section S4.3.

Table 4
Electronic couplings, energy differences and geometrical parameters for our designed covalent dimers of DATFQ (Fig. 5). The reported electronic couplings and energy differences were computed at the MR-DDC2 level, after shifting the following state energies (diagonal elements): S_1S_0 and S_0S_1 (−0.32 eV), TT (−0.48 eV), A^-B^+ and A^+B^- (−0.32 eV). These energy shifts were determined by comparison of the MR-DDC2(6,4) energies of S_1 and T_1 for the monomer with the corresponding reference (TD-)DFT energies (Table S10). The complete MR-DDC2 electronic Hamiltonian matrices are provided in Table S11.

Dimer	R[a]	r[b]	ϕ[c]	Coupling (meV)		Energy gap (meV)[f]			
	(Å)	(Å)	(deg.)	F[d]	D[e]	$S_2^*-S_1^*$	$TT-S_1^*$	$TT-S_2^*$	$CT_1-S_2^*$
SS-CH_2	2.786	0.839	3.3	111.1	22.7	363.3	491.7	128.4	84.1
RS-CH_2	2.826	1.025	0.0	74.4	22.8	341.4	349.1	7.7	150.2
SS-CH_2O	3.417	1.325	23.5	43.2	9.2	195.9	333.6	137.7	603.0
RS-CH_2O	4.329	0.485	0.0	7.0	1.3	156.2	129.8	−26.5	970.5
SS-OCH_2	4.171	0.997	3.0	32.3	6.6	188.9	338.0	149.2	711.6
RS-OCH_2	3.851	1.165	0.0	17.7	0.2	205.3	645.5	440.2	765.3

[a] R is the stacking distance between monomers and is defined as the average distance (in Å) between the centroid of one monomer and its projection to the best-fit plane of the other monomer.

[b] r is the slip distance between monomers and is defined as the average distance (in Å) between the centroid of one monomer and the centroid projection of the other monomer to the best-fit plane of the first monomer.

[c] ϕ is the tilting angle and is defined as the angle (in degrees) between the normal vectors of the best-fit planes for the two monomers.

[d] F is defined as $\sqrt{\langle S_1S_0|\hat{H}_{el}^{eff}|TT\rangle^2+\langle S_0S_1|\hat{H}_{el}^{eff}|TT\rangle^2}$ (Eq. (1)), and quantifies the effective coupling of the S_1S_0 and S_0S_1 states with TT, including the effect of CT states A^-B^+ and A^+B^-.

[e] D is defined as $\sqrt{\langle S_1S_0|\hat{H}_{el}|TT\rangle^2+\langle S_0S_1|\hat{H}_{el}|TT\rangle^2}$, and quantifies the direct coupling of the S_1S_0 and S_0S_1 states with TT.

[f] Energy gap between states i and j (i.e. $i-j$) defined as E_i-E_j. A positive gap indicates that state i is above state j, while a negative gap means that i lies below j. State notation: S_2^*, S_1^*, higher- (bright) and lower-energy (dark) excitonic states, respectively; TT, double triplet state; CT_1, lower-energy state of charge transfer character.

A more thorough assessment of the SF suitability for SS-CH_2 and RS-CH_2 requires to perform simulations of the nonadiabatic excited-state dynamics, as we have already done for dimers **D1** and **D2** of ML-DPBF [56]. As a first step towards the realization of dynamics simulations, we have reoptimized the AM1 [54] semiempirical parameters for dimers SS-CH_2 and RS-CH_2, using our computed (TD-)DFT and MR-DDC2 data as target values for the reparametrization (see Section S2.2 for details).

With the new semiempirical parameters, our FOMO-CI scheme was used to optimize the geometries of dimers SS-CH_2 and RS-CH_2 for their adiabatic S_0 and S_1 states (referred to as S_0^d and S_1^d, respectively). For both dimers, at the S_1^d minimum the TT state is the lowest excited state, the TT adiabatic transition energy being 2.75 eV for SS-CH_2 and 2.44 eV for RS-CH_2 (Table S15). Moreover, at the same geometry, the energy gap between TT and the S_1^* state is 0.31 eV for SS-CH_2 and 0.75 eV for RS-CH_2. These data indicate that in both dimers the SF energetics is favorable, confirming the outlook provided by the monomer state energies [47].

3.3. Computational details of design II

The ground state geometries of our designed covalent dimers of DATFQ were optimized at the DFT level, using the M06-2X functional [61] and the TZVP basis set [62], as already done for the DATFQ

monomer in our previous work [47]. No symmetry constraint was imposed in the geometry optimizations and Hessian calculations were carried out to check if the optimized geometries were energy minima.

At the M06-2X/TZVP optimized dimeric geometries, electronic structure calculations were performed using a multireference configuration interaction (MR-CI) technique devised to treat large systems [63–65]. The method exploits the localization of molecular orbitals (MOs) [66] to reduce both the determinant basis and the number of two electron integrals that contribute to the CI matrix. In our calculations, the MR-CI adiabatic states were computed on top of state-averaged (SA) complete active space self consistent field (CASSCF) calculations, using the difference dedicated configuration interaction scheme DDC2 [67,68]. In the DDC2 approach all possible single excitations out of the reference complete active space (CAS) are taken into account, in addition to all double excitations from the occupied to the active MOs and from the active to the virtual MOs. Moreover, in our approach the determinant basis is further reduced by applying a selection procedure, based on localized MOs, to the aforementioned set of singly and doubly excited determinants [65] (see Section S3 for more details).

All the MR-DDC2 calculations for our dimers of DATFQ were performed using the basis set ANO-L [69,70], contracted to $3s2p1d$ for C, N and O, $3s2p$ for F, and $2s$ for H. Moreover, in both the SA-CASSCF and the subsequent MR-CI calculations, we computed the six low-lying singlet electronic states, using an orbital active space of 12 electrons in 8 orbitals, i.e. CAS(12,8). This active space, as well as the DDC2 scheme, was selected by comparing the S_1 and T_1 excitation energies for the DATFQ monomer computed at different MR-CI levels with the (TD-)DFT reference energies [47] (see Table S10).

The electronic couplings and energy gaps between states were computed at the MR-DDC2 level using a diabatization procedure similar to the one employed for the ML-DPBF dimers (Section 2). In particular, after computing the energies and wavefunctions for the 6 low-lying singlet adiabatic states of our DATFQ dimers, (quasi-)diabatic states were defined by applying a unitary transformation to the adiabatic states, so as to maximize the overlaps between the diabatic wavefunctions and a set of 6 reference states [46]. The latter are the following diabatic prototypes: the ground state, S_0S_0, the localized excitations S_1S_0 and S_0S_1, the double triplet state, TT, the charge transfer (CT) states A^-B^+ and A^+B^- (see Figure S7 for a schematic representation).

As for the dimers of ML-DPBF (see end of Section 2.3), the effective electronic couplings between S_1S_0/S_0S_1 and TT were computed by defining an effective Hamiltonian matrix in which the model space is spanned by S_1S_0, S_0S_1 and TT, and the outer space is defined by the CT states A^-B^+, A^+B^- [46]. Moreover, the excitonic states S_1^* and S_2^*, and CT_1 and CT_2 were computed by diagonalizing separately the electronic Hamiltonian matrix blocks of the localized excitations, S_1S_0 and S_0S_1, and the CT states, A^-B^+ and A^+B^-, respectively.

All the M06-2X/TZVP geometry optimizations were performed with Gaussian09 revision A.02 [71]. The MR-DDC2 calculations were carried out using the Cost Package [72], interfaced with Molcas 7, revision 7.8 [73].

4. Conclusions

We have presented two different computational approaches to design novel covalently bound dimers for singlet fission (SF). Both approaches aim at maximizing the effective electronic coupling between the initial singlet S^* and the double triplet state TT, by tuning the interaction between the two monomers. Note that the effective couplings take into account the S^*-TT interactions through the charge transfer states, which are of major importance in all the cases here considered.

Our first design is based on a search for the optimal mutual dispositions of two slip-stacked chromophores, followed by the covalent connection of the chromophore units so as to attain the optimized dimeric arrangements. This approach is suitable for SF chromophores having a planar structure and several possible connecting sites. By applying our design to the methylene-locked 1,3-diphenyl-isobenzofuran (ML-DPBF) compound, we obtained several promising covalent dimers, in which the mutual dispositions of chromophores are very close to the corresponding target dimeric arrangements. The characterization of our proposed dimers of ML-DPBF showed that in all our designed systems the S^*-TT effective and direct couplings are quite large and the energy gap between the bright excitonic state S_2^* and TT is very small. The suitability for SF of two of these dimers of ML-DPBF, namely **D1** and **D2**, was already further investigated in our earlier published work, in which nonadiabatic dynamics simulations indicated that both dimers undergo intramolecular SF in the sub-picosecond time scale, with SF quantum yields close to 200% [56].

In our second design, we considered several ways to covalently connect the two chromophores, using different linkers. Next, the candidate dimers were characterized and the most promising dimers for SF were identified. This approach can be applied to SF chromophores featuring a small number of connecting sites and a limited set of possible target dimeric arrangements for the covalent connection. As an example, we considered covalent dimers of a diamino-trifluoroquinone (DATFQ) chromophore. Our approach allowed to design several candidate dimers of DATFQ and to identify the most promising ones for SF, namely dimers SS-CH_2 and RS-CH_2, which show the largest S^*-TT effective and direct couplings, as well as a favorable SF energetics. Simulations of the nonadiabatic excited-state dynamics are planned in order to better assess the suitability for SF of dimers SS-CH_2 and RS-CH_2.

CRediT authorship contribution statement

Davide Accomasso: Writing – original draft, Investigation, Formal analysis, Data curation, Conceptualization. **Nadia Ben Amor:** Writing – review & editing, Methodology, Investigation. **Maurizio Persico:** Writing – review & editing, Supervision, Project administration, Investigation, Funding acquisition, Conceptualization. **Giovanni Granucci:** Writing – review & editing, Supervision, Project administration, Investigation, Funding acquisition, Conceptualization.

Declaration of competing interest

The authors declare that they have no known competing financial interests or personal relationships that could have appeared to influence the work reported in this paper.

Data availability

Data will be made available on request.

Acknowledgments

We acknowledge the financial support of the ITN MSC Actions (grant ITN-EJD-642294-TCCM).

Appendix A. Supplementary data

Supplementary material related to this article can be found online at https://doi.org/10.1016/j.jphotochem.2023.114836.

References

[1] M.B. Smith, J. Michl, Singlet fission, Chem. Rev. 110 (2010) 6891–6936.

[2] M.B. Smith, J. Michl, Recent advances in singlet fission, Annu. Rev. Phys. Chem. 64 (1) (2013) 361–386.

[3] A. Japahuge, T. Zeng, Theoretical studies of singlet fission: Searching for materials and exploring mechanisms, ChemPlusChem 83 (4) (2018) 146–182.

[4] D. Casanova, Theoretical modeling of singlet fission, Chem. Rev. 118 (15) (2018) 7164–7207.

[5] A. Rao, M.W.B. Wilson, J.M. Hodgkiss, S. Albert-Seifried, H. Bässler, R.H. Friend, Exciton fission and charge generation via triplet excitons in pentacene/C60 bilayers, J. Am. Chem. Soc. 132 (36) (2010) 12698–12703.

[6] M.W.B. Wilson, A. Rao, J. Clark, R.S.S. Kumar, D. Brida, G. Cerullo, R.H. Friend, Ultrafast dynamics of exciton fission in polycrystalline pentacene, J. Am. Chem. Soc. 133 (31) (2011) 11830–11833.

[7] W. Shockley, H.J. Queisser, Detailed balance limit of efficiency of p-n junction solar cells, J. Appl. Phys. 32 (3) (1961) 510–519.

[8] M.C. Hanna, A.J. Nozik, Solar conversion efficiency of photovoltaic and photoelectrolysis cells with carrier multiplication absorbers, J. Appl. Phys. 100 (7) (2006) 1–8.

[9] J.C. Johnson, A.J. Nozik, J. Michl, The role of chromophore coupling in singlet fission, Acc. Chem. Res. 46 (6) (2013) 1290–1299.

[10] N. Monahan, X.-Y. Zhu, Charge transfer-mediated singlet fission, Annu. Rev. Phys. Chem. 66 (1) (2015) 601–618.

[11] G.B. Piland, C.J. Bardeen, How morphology affects singlet fission in crystalline tetracene, J. Phys. Chem. Lett. 6 (10) (2015) 1841–1846.

[12] R.D. Pensack, A.J. Tilley, S.R. Parkin, T.S. Lee, M.M. Payne, D. Gao, A.A. Jahnke, D.G. Oblinsky, P.-F. Li, J.E. Anthony, D.S. Seferos, G.D. Scholes, Exciton delocalization drives rapid singlet fission in nanoparticles of acene derivatives, J. Am. Chem. Soc. 137 (21) (2015) 6790–6803.

[13] J.L. Ryerson, J.N. Schrauben, A.J. Ferguson, S.C. Sahoo, P. Naumov, Z. Havlas, J. Michl, A.J. Nozik, J.C. Johnson, Two thin film polymorphs of the singlet fission compound 1,3-diphenylisobenzofuran, J. Phys. Chem. C 118 (23) (2014) 12121–12132.

[14] H. Tamura, M. Huix-Rotllant, I. Burghardt, Y. Olivier, D. Beljonne, First-principles quantum dynamics of singlet fission: Coherent versus thermally activated mechanisms governed by molecular π stacking, Phys. Rev. Lett. 115 (2015) 107401.

[15] N.V. Korovina, N.F. Pompetti, J.C. Johnson, Lessons from intramolecular singlet fission with covalently bound chromophores, J. Chem. Phys. 152 (4) (2020) 040904.

[16] A.M. Müller, Y.S. Avlasevich, K. Müllen, C.J. Bardeen, Evidence for exciton fission and fusion in a covalently linked tetracene dimer, Chem. Phys. Lett. 421 (4) (2006) 518–522.

[17] A.M. Müller, Y.S. Avlasevich, W.W. Schoeller, K. Müllen, C.J. Bardeen, Exciton fission and fusion in bis(tetracene) molecules with different covalent linker structures, J. Am. Chem. Soc. 129 (46) (2007) 14240–14250.

[18] P.J. Vallett, J.L. Snyder, N.H. Damrauer, Tunable electronic coupling and driving force in structurally well-defined tetracene dimers for molecular singlet fission: A computational exploration using density functional theory, J. Phys. Chem. A 117 (42) (2013) 10824–10838.

[19] H. Liu, V.M. Nichols, L. Shen, S. Jahansouz, Y. Chen, K.M. Hanson, C.J. Bardeen, X. Li, Synthesis and photophysical properties of a "face-to-face" stacked tetracene dimer, Phys. Chem. Chem. Phys. 17 (2015) 6523–6531.

[20] N.V. Korovina, S. Das, Z. Nett, X. Feng, J. Joy, R. Haiges, A.I. Krylov, S.E. Bradforth, M.E. Thompson, Singlet fission in a covalently linked cofacial alkynyltetracene dimer, J. Am. Chem. Soc. 138 (2) (2016) 617–627.

[21] X. Feng, D. Casanova, A.I. Krylov, Intra- and intermolecular singlet fission in covalently linked dimers, J. Phys. Chem. C 120 (34) (2016) 19070–19077.

[22] T. Yamakado, S. Takahashi, K. Watanabe, Y. Matsumoto, A. Osuka, S. Saito, Conformational planarization versus singlet fission: Distinct excited-state dynamics of cyclooctatetraene-fused acene dimers, Angew. Chem. Int. Ed. 57 (19) (2018) 5438–5443.

[23] Y. Matsui, S. Kawaoka, H. Nagashima, T. Nakagawa, N. Okamura, T. Ogaki, E. Ohta, S. Akimoto, A. Sato-Tomita, S. Yagi, Y. Kobori, H. Ikeda, Exergonic intramolecular singlet fission of an adamantane-linked tetracene dyad via twin quintet multiexcitons, J. Phys. Chem. C 123 (31) (2019) 18813–18823.

[24] K. Okada, M. Nakano, H. Miyamoto, H. Nakazawa, Y. Uetake, H. Sakurai, Theoretical study on singlet fission dynamics in sumanene-fused acene dimers, J. Phys. Chem. C 124 (36) (2020) 19499–19507.

[25] J. Zirzlmeier, D. Lehnherr, P.B. Coto, E.T. Chernick, R. Casillas, B.S. Basel, M. Thoss, R.R. Tykwinski, D.M. Guldi, Singlet fission in pentacene dimers, Proc. Natl. Acad. Sci. 112 (17) (2015) 5325–5330.

[26] S.N. Sanders, E. Kumarasamy, A.B. Pun, M.T. Trinh, B. Choi, J. Xia, E.J. Taffet, J.Z. Low, J.R. Miller, X. Roy, X.-Y. Zhu, M.L. Steigerwald, M.Y. Sfeir, L.M. Campos, Quantitative intramolecular singlet fission in bipentacenes, J. Am. Chem. Soc. 137 (28) (2015) 8965–8972.

[27] S. Lukman, A.J. Musser, K. Chen, S. Athanasopoulos, C.K. Yong, Z. Zeng, Q. Ye, C. Chi, J.M. Hodgkiss, J. Wu, R.H. Friend, N.C. Greenham, Tuneable singlet exciton fission and triplet-triplet annihilation in an orthogonal pentacene dimer, Adv. Funct. Mater. 25 (34) (2015) 5452–5461.

[28] J. Zirzlmeier, R. Casillas, S.R. Reddy, P.B. Coto, D. Lehnherr, E.T. Chernick, I. Papadopoulos, M. Thoss, R.R. Tykwinski, D.M. Guldi, Solution-based intramolecular singlet fission in cross-conjugated pentacene dimers, Nanoscale 8 (2016) 10113–10123.

[29] T. Sakuma, H. Sakai, Y. Araki, T. Mori, T. Wada, N.V. Tkachenko, T. Hasobe, Long-lived triplet excited states of bent-shaped pentacene dimers by intramolecular singlet fission, J. Phys. Chem. A 120 (11) (2016) 1867–1875.

[30] E.G. Fuemmeler, S.N. Sanders, A.B. Pun, E. Kumarasamy, T. Zeng, K. Miyata, M.L. Steigerwald, X.-Y. Zhu, M.Y. Sfeir, L.M. Campos, N. Ananth, A direct mechanism of ultrafast intramolecular singlet fission in pentacene dimers, ACS Cent. Sci. 2 (5) (2016) 316–324.

[31] C. Hetzer, D.M. Guldi, R.R. Tykwinski, Frontispiece: Pentacene dimers as a critical tool for the investigation of intramolecular singlet fission, Chem. Eur. J. 24 (33) (2018).

[32] I. Papadopoulos, Y. Gao, C. Hetzer, R.R. Tykwinski, D.M. Guldi, Singlet fission in enantiomerically pure pentacene dimers, ChemPhotoChem 4 (10) (2020) 5168–5174.

[33] J.C. Johnson, A. Akdag, M. Zamadar, X. Chen, A.F. Schwerin, I. Paci, M.B. Smith, Z. Havlas, J.R. Miller, M.A. Ratner, A.J. Nozik, J. Michl, Toward designed singlet fission: Solution photophysics of two indirectly coupled covalent dimers of 1,3-diphenylisobenzofuran, J. Phys. Chem. B 117 (16) (2013) 4680–4695.

[34] A. Akdag, A. Wahab, P. Beran, L. Rulíšek, P.I. Dron, J. Ludvík, J. Michl, Covalent dimers of 1,3-diphenylisobenzofuran for singlet fission: Synthesis and electrochemistry, J. Org. Chem. 80 (1) (2015) 80–89.

[35] J.N. Schrauben, A. Akdag, J. Wen, Z. Havlas, J.L. Ryerson, M.B. Smith, J. Michl, J.C. Johnson, Excitation localization/delocalization isomerism in a strongly coupled covalent dimer of 1,3-diphenylisobenzofuran, J. Phys. Chem. A 120 (20) (2016) 3473–3483.

[36] E.A. Margulies, L.E. Shoer, S.W. Eaton, M.R. Wasielewski, Excimer formation in cofacial and slip-stacked perylene-3, 4:9, 10-bis(dicarboximide) dimers on a redox-inactive triptycene scaffold, Phys. Chem. Chem. Phys. 16 (2014) 23735–23742.

[37] E.A. Margulies, C.E. Miller, Y. Wu, L. Ma, G.C. Schatz, R.M. Young, M.R. Wasielewski, Enabling singlet fission by controlling intramolecular charge transfer in π-stacked covalent terrylenediimide dimers, Nature Chem. 8 (2016) 1120–1125.

[38] W. Ni, G.G. Gurzadyan, J. Zhao, Y. Che, X. Li, L. Sun, Singlet fission from upper excited electronic states of cofacial perylene dimer, J. Phys. Chem. Lett. 10 (10) (2019) 2428–2433.

[39] O. Varnavski, N. Abeyasinghe, J. Aragó, J.J. Serrano-Pérez, E. Ortí, J.T. López Navarrete, K. Takimiya, D. Casanova, J. Casado, T. Goodson, High yield ultrafast intramolecular singlet exciton fission in a quinoidal bithiophene, J. Phys. Chem. Lett. 6 (8) (2015) 1375–1384.

[40] A.D. Chien, A.R. Molina, N. Abeyasinghe, O.P. Varnavski, T. Goodson, P.M. Zimmerman, Structure and dynamics of the ^{1}(TT) state in a quinoidal bithiophene: Characterizing a promising intramolecular singlet fission candidate, J. Phys. Chem. C 119 (51) (2015) 28258–28268.

[41] T. Zeng, P. Goel, Design of small intramolecular singlet fission chromophores: An azaborine candidate and general small size effects, J. Phys. Chem. Lett. 7 (7) (2016) 1351–1358.

[42] T. Zeng, Through-linker intramolecular singlet fission: General mechanism and designing small chromophores, J. Phys. Chem. Lett. 7 (21) (2016) 4405–4412.

[43] R. Montero, V. Martínez-Martínez, A. Longarte, N. Epelde-Elezcano, E. Palao, I. Lamas, H. Manzano, A.R. Agarrabeitia, I. López Arbeloa, M.J. Ortiz, I. Garcia-Moreno, Singlet fission mediated photophysics of BODIPY dimers, J. Phys. Chem. Lett. 9 (3) (2018) 641–646.

[44] J. Choi, S. Kim, M. Ahn, J. Kim, D.W. Cho, D. Kim, S. Eom, D. Im, Y. Kim, S.H. Kim, K.-R. Wee, H. Ihee, Singlet fission dynamics modulated by molecular configuration in covalently linked pyrene dimers, Anti- and Syn-1,2-di(pyrenyl)benzene, Commun. Chem. 6 (16) (2023).

[45] O. Millington, S. Montanaro, A. Leventis, A. Sharma, S.A. Dowland, N. Sawhney, K.J. Fallon, W. Zeng, D.G. Congrave, A.J. Musser, A. Rao, H. Bronstein, Soluble diphenylhexatriene dimers for intramolecular singlet fission with high triplet energy, J. Am. Chem. Soc. 145 (4) (2023) 2499–2510.

[46] D. Accomasso, M. Persico, G. Granucci, Diabatization by localization in the framework of configuration interaction based on floating occupation molecular orbitals (FOMO-CI), ChemPhotoChem 3 (9) (2019) 933–944.

[47] D. Accomasso, M. Persico, G. Granucci, Computational design of singlet fission biradicaloid chromophores, J. Photochem. Photobiol. A: Chem. 427 (2022) 113807.

[48] J.A. Nelder, R. Mead, A simplex method for function minimization, Comput. J. 7 (4) (1965) 308–313.

[49] E.A. Buchanan, J. Michl, Optimal arrangements of 1, 3-diphenylisobenzofuran molecule pairs for fast singlet fission, Photochem. Photobiol. Sci. 18 (2019) 2112–2124.

[50] E.A. Buchanan, J.C. Johnson, M. Tan, J. Kaleta, A.G. Shtukenberg, G. Bateman, J.B. Benedict, S. Kobayashi, J. Wen, B. Kahr, I. Císařová, J. Michl, Competing singlet fission and excimer formation in solid fluorinated 1,3-diphenylisobenzofurans, J. Phys. Chem. C 125 (49) (2021) 27058–27071.

[51] Q. Ge, M. Head-Gordon, Energy decomposition analysis for excimers using absolutely localized molecular orbitals within time-dependent density functional theory and configuration interaction with single excitations, J. Chem. Theory Comput. 14 (10) (2018) 5156–5168.

[52] G. Granucci, M. Persico, A. Toniolo, Direct semiclassical simulation of photochemical processes with semiempirical wave functions, J. Chem. Phys. 114 (24) (2001) 10608–10615.

[53] G. Granucci, A. Toniolo, Molecular gradients for semiempirical CI wavefunctions with floating occupation molecular orbitals, Chem. Phys. Lett. 325 (2000) 79–85.

[54] M.J.S. Dewar, E.G. Zoebisch, E.F. Healy, J.J.P. Stewart, AM1: A new general purpose quantum mechanical molecular model, J. Am. Chem. Soc. 107 (13) (1985) 3902–3909.

[55] W.L. Jorgensen, D.S. Maxwell, J. Tirado-Rives, Development and testing of the OPLS all-atom force field on conformational energetics and properties of organic liquids, J. Am. Chem. Soc. 118 (45) (1996) 11225–11236.
[56] D. Accomasso, G. Granucci, M. Persico, Singlet fission in covalent dimers of methylene-locked 1, 3-diphenyl-isobenzofuran: semiclassical simulations of nonadiabatic dynamics, J. Mater. Chem. A 9 (2021) 21897–21909.
[57] J.J.P. Stewart, MOPAC2002, Fujitsu Limited, Tokyo, Japan, 2002.
[58] J. Wen, Z. Havlas, J. Michl, Captodatively stabilized biradicaloids as chromophores for singlet fission, J. Am. Chem. Soc. 137 (1) (2015) 165–172.
[59] J. Wen, M. Turowski, P.I. Dron, J. Chalupský, R. Grotjahn, T.M. Maier, S.M. Fatur, Z. Havlas, J.C. Johnson, M. Kaupp, J. Michl, Electronic states of 2,3-diamino-1,4-naphthoquinone and its N-alkylated derivatives, J. Phys. Chem. C 124 (1) (2020) 60–69.
[60] D. Accomasso, G. Granucci, R.W.A. Havenith, M. Persico, Testing new chromophores for singlet fission: A computational protocol applied to 2,3-diamino-1,4-benzoquinone, Chem. Phys. 515 (2018) 635–642.
[61] Y. Zhao, D.G. Truhlar, The M06 suite of density functionals for main group thermochemistry, thermochemical kinetics, noncovalent interactions, excited states, and transition elements: two new functionals and systematic testing of four M06-class functionals and 12 other functionals, Theor. Chem. Acc. 120 (2008) 215–241.
[62] A. Schäfer, C. Huber, R. Ahlrichs, Fully optimized contracted Gaussian basis sets of triple zeta valence quality for atoms Li to Kr, J. Chem. Phys. 100 (8) (1994) 5829–5835.
[63] B. Bories, D. Maynau, M.-L. Bonnet, Selected excitation for CAS-SDCI calculations, J. Comput. Chem. 28 (3) (2007) 632–643.
[64] N. Ben Amor, F. Bessac, S. Hoyau, D. Maynau, Direct selected multireference configuration interaction calculations for large systems using localized orbitals, J. Chem. Phys. 135 (1) (2011) 014101.
[65] C. Chang, C.J. Calzado, N. Ben Amor, J. Sanchez Marin, D. Maynau, Multi-scale multireference configuration interaction calculations for large systems using localized orbitals: Partition in zones, J. Chem. Phys. 137 (10) (2012) 104102.
[66] D. Maynau, S. Evangelisti, N. Guihéry, C.J. Calzado, J.-P. Malrieu, Direct generation of local orbitals for multireference treatment and subsequent uses for the calculation of the correlation energy, J. Chem. Phys. 116 (23) (2002) 10060–10068.
[67] J. Miralles, J.-P. Daudey, R. Caballol, Variational calculation of small energy differences. The singlet-triplet gap in $[Cu_2Cl_6]^{2-}$, Chem. Phys. Lett. 198 (6) (1992) 555–562.
[68] J. Miralles, O. Castell, R. Caballol, J.-P. Malrieu, Specific CI calculation of energy differences: Transition energies and bond energies, Chem. Phys. 172 (1) (1993) 33–43.
[69] P.-O. Widmark, P.A. Malmqvist, B.O. Roos, Density matrix averaged atomic natural orbital (ANO) basis sets for correlated molecular wave functions - First row atoms, Theor. Chim. Acta 77 (1990) 291–306.
[70] P.-O. Widmark, B.J. Persson, B.O. Roos, Density matrix averaged atomic natural orbital (ANO) basis sets for correlated molecular wave function - Second row atoms, Theor. Chim. Acta 79 (1991) 419–432.
[71] J.M. Frisch, W.G. Trucks, B.H. Schlegel, E.G. Scuseria, A.M. Robb, R.J. Cheeseman, G. Scalmani, V. Barone, B. Mennucci, A.G. Petersson, H. Nakatsuji, M. Caricato, X. Li, P.H. Hratchian, F.A. Izmaylov, J. Bloino, G. Zheng, L.J. Sonnenberg, M. Hada, M. Ehara, K. Toyota, R. Fukuda, J. Hasegawa, M. Ishida, T. Nakajima, Y. Honda, O. Kitao, H. Nakai, T. Vreven, A.J. Montgomery Jr., E.J. Peralta, F. Ogliaro, M. Bearpark, J.J. Heyd, E. Brothers, N.K. Kudin, N.V. Staroverov, R. Kobayashi, J. Normand, K. Raghavachari, A. Rendell, C.J. Burant, S.S. Iyengar, J. Tomasi, M. Cossi, N. Rega, M.J. Millam, M. Klene, E.J. Knox, B.J. Cross, V. Bakken, C. Adamo, J. Jaramillo, R. Gomperts, E.R. Stratmann, O. Yazyev, J.A. Austin, R. Cammi, C. Pomelli, W.J. Ochterski, L.R. Martin, K. Morokuma, G.V. Zakrzewski, A.G. Voth, P. Salvador, J.J. Dannenberg, S. Dapprich, D.A. Daniels, Ö. Farkas, B.J. Foresman, V.J. Ortiz, J. Cioslowski, J.D. Fox, Gaussian 09 (Gaussian, Inc., Wallingford CT), 2009.
[72] D. Maynau, N. Ben Amor, J.-V. Pitarch-Ruiz, A. Monari, H. S., Cost package, 2020, http://github.com/LCPQ/Cost_package. (Accessed 18 November 2020).
[73] F. Aquilante, L. De Vico, N. Ferré, G. Ghigo, P.-A. Malmqvist, P. Neogrády, T.B. Pedersen, M. Pitoňák, M. Reiher, B.O. Roos, L. Serrano-Andrés, M. Urban, V. Veryazov, R. Lindh, MOLCAS 7: The next generation, J. Comput. Chem. 31 (1) (2010) 224–247.